Multipath Cluster Analysis for Device-to-Device Terahertz Outdoor Measurements

 $Zihang\ Cheng^*,\ Naveed\ A.\ Abbasi^*,\ Jorge\ Gomez-Ponce^{*\dagger},\ Jianzhong\ (Charlie)\ Zhang^{\ddagger},\ and\ Andreas\ F.\ Molisch^*$

*University of Southern California, Los Angeles, CA, USA †ESPOL Polytechnic University, Guayaquil, Ecuador

‡Samsung Research America, Richardson, TX, USA

Email: {zihangch, nabbasi, gomezpon, molisch}@usc.edu, jianzhong.z@samsung.com

Abstract—Since the terahertz frequency band (0.1-1 THz) has attracted considerable attention for the upcoming sixthgeneration (6G) wireless communication systems, accurate models for multipath propagation in this frequency range need to be established. Such models advantageously use the fact that multipath components (MPCs) occur typically in clusters, i.e., groups of MPCs that have similar delays and angles. In this paper, we first analyze the limitations of a widely used clustering algorithm, Kernel-Power-Density (KPD), in evaluating an extensive THz outdoor measurement campaign at 145-146 GHz, particularly its inability to detect small clusters. We introduce a modified version, which we term multi-level KPD (ML-KPD), iteratively applying KPD to detect whether a cluster determined in the previous round is made up of multiple clusters. We first apply the method to synthetic channels to demonstrate its efficacy and select suitable values for the adaptive hyperparameters. Then, multi-level KPD is applied to our channel measurements in lineof-sight (LOS) and non-line-of-sight (NLOS) environments to determine statistics for the number of clusters and the cluster

Index Terms—Channel measurement, clustering, device-to-device, outdoor, THz

I. Introduction

A number of new and upcoming applications require data rates that are beyond the capabilities of our current fifthgeneration (5G) wireless communication systems. The use of spectrum in the terahertz¹ frequency band (0.1–1 THz) is a promising avenue towards meeting those requirements [1], [2]. Since both the fundamental performance limits and the practical performance of any wireless system are determined by the characteristics of the channels it operates in, we need new channel models that accurately reflect these characteristics in the new frequency bands. As with any channel model, they need to be based on, or verified by, accurate measurements (i.e., *channel sounding*) [3], [4]. Over the past years, several such measurements have been performed [5].

These measurements (e.g., [6], [7]) show that–similar to lower frequency bands–the multipath components (MPCs) in THz channels occur in clusters, *i.e.*, a group of MPCs that have similar delay and angular parameters, while significantly different from those of MPCs not part of the cluster.² Clustering not only simplifies the channel model, allowing to factor

¹The 0.1–0.3 THz range is also often called the sub-THz regime. We use here THz for the whole band for the purpose of more compact notation.

²This is the common definition of clusters both in the scientific literature since at least the 1980s [8], and in standardized models such as the COST 259/273/2100 model [9], [10]. The 3GPP channel model [11] uses a somewhat different definition in which all MPCs in a cluster have exactly the same delay and only the angles are different (more recent version includes a splitting of the delays into two different values).

the MPC statistics into intra- and inter-cluster statistics, but also describes an effect that is important for system behavior, determining, e.g., limitations of analog beamforming.

Because of its importance, a wide variety of clustering algorithms have been developed, often drawing inspiration from related problems in computer science [3]. The most popular ones include the K-Power-Means [12], and Density-Based Spatial Clustering of Applications with Noise (DB-SCAN) [13] algorithm. More recently, the Kernel-Power-Density (KPD) algorithm [14] was proposed. It has the advantage that-in contrast to K-Power-Means-it depends neither on the initialization of clusters, nor location and the number of clusters, and significantly outperforms DBSCAN [14] in terms of widely used quality criteria for clustering (Fmeasure and silhouette coefficient). However, the performance of KPD clustering relies on the hyperparameter selection, especially the number of nearest neighbors taken into account in the density computation procedure. As we observed during an analysis of a large-scale outdoor channel measurement campaign [15], it tends to insufficiently separate MPCs from different clusters.

Our main contributions in this paper are: (i) we demonstrate the limitations of KPD in analyzing our real-world outdoor device-to-device (D2D)³ measurement campaigns at 145 GHz; (ii) we develop a new algorithm, multi-level KPD, that overcomes these limitations; and (iii) we use our new algorithm to analyze the cluster statistics, in particular the number of clusters, cluster delay spread (DS), and cluster angular spread (AS), of our measurements.

While terahertz frequencies offer larger bandwidth, we conjecture that the clustering behavior observed in THz channels is not fundamentally different from that in lower-frequency bands. The main motivation for focusing on THz channels in this paper is the real-world measurements analyzed here. The multi-level KPD algorithm is designed to overcome limitations in existing methods and improve cluster analysis in a variety of scenarios and frequency bands.

II. MEASUREMENTS, SIGNAL MODEL, AND MPC EXTRACTION

A. Measurement Locations

For the convenience of the reader, we briefly summarize the measurement campaign; a detailed sounder and measurement

³In military communication, D2D communication is particularly important for direct communications between soldiers, or between combat vehicles.

description can be found in [15]. The measurements of both line-of-sight (LOS) and non-line-of-sight (NLOS) scenarios were conducted in two distinct locations: (i) an intersection of two roads, and (ii) a quad surrounded by vegetation and buildings. The *intersection* has buildings on three corners, and a sport playground at the remaining one, with trees and bushes nearby and along the streets. The *quad* environment on the campus of USC is surrounded by multi-story concrete buildings. It includes an open area interspersed with concrete pillars and a courtyard with tables, umbrellas, lamp poles, bushes, and a fountain. The measurements were done for a D2D setup, with both transmitter (Tx) and receiver (Rx) antennas about 1.5 m above ground. In total, there are 21 LOS and 17 NLOS Tx/Rx location pairs.

B. Signal Model

The channel response can be expressed as the superposition of MPCs that in the far field of antennas can be modeled as planar waves [16]. The MPCs are characterized by a set of parameters, i.e., complex amplitude, direction of arrival (DoA), direction of departure (DoD), and propagation delay. The multiple-input multiple-output (MIMO) transfer function matrix of the channel between $N_{\rm T}$ Tx antennas and $N_{\rm R}$ Rx antennas at a specific frequency point, f_k , can be expressed in terms of these MPC parameters [4]. Note that this matrix is actually observed during measurements, and its evaluation by Fourier methods has a resolution that is limited by the aperture in the different domains (bandwidth, array apertures at Tx and Rx). With sufficiently high resolution in all parametric domains [14], the formation of clusters in the different parametric domains can also be observed in this matrix [17]; alternatively, high resolution parameter estimation can provide appropriate resolution [4]. Therefore, the clustered signal model can be expressed as

$$\mathbf{H}(f_k) = \sum_{c=1}^{N_{\rm C}} \sum_{p=1}^{N_c} \gamma_{cp} \tilde{\mathbf{g}}_{\rm R}(\mathbf{\Omega}_{{\rm R},cp}) \tilde{\mathbf{g}}_{\rm T}^T(\mathbf{\Omega}_{{\rm T},cp}) e^{-j2\pi f_k \tau_{cp}} + \mathbf{N},$$
(1)

where γ , $\Omega_{\rm R}$, $\Omega_{\rm T}$, and τ are complex amplitude, DoA, DoD and propagation delay, respectively, of the p-th MPC in the c-th cluster. $N_{\rm C}$ is the total number of clusters existing in the channel, and N_c refers to the number of MPCs within the c-th cluster. The calibrated array patterns, $\tilde{\mathbf{g}}_{\rm R}(\Omega_{\rm R}) \in \mathbb{C}^{N_{\rm R} \times 1}$ and $\tilde{\mathbf{g}}_{\rm T}(\Omega_{\rm T}) \in \mathbb{C}^{N_{\rm T} \times 1}$, express the array response in a certain direction. The additive noise, $\mathbf{N} \in \mathbb{C}^{N_{\rm R} \times N_{\rm T}}$, follows a zeromean circularly symmetric complex Gaussian distribution and is independent between antennas and frequencies.

C. MPC Tap Extraction

For the current measurements, the transfer function matrix is measured by sweeping the frequency using a Vector Network Analyzer (VNA), while horn antennas at Tx and Rx are rotated by precision stepper motors into different directions, scanning the azimuth with spacing 10°. While other measurement principles can be applied as well [3], the subsequent processing remains the same.

Each element of the channel matrix in (1) is the convolution between MPCs and the antenna array responses at the corresponding directions, which cannot be easily decoupled (high-resolution parameter estimation for this decoupling will be subject of our future work). Consequently, the angle-delay power spectrum (ADPS) is regarded as the indicator in this paper on which delay and angular *bins* the MPC clusters locate at.

We first form the ADPS on a grid in parameter space, which can be expressed as

$$P_{\text{ADPS}}(\tau, \phi_{\text{R}}, \phi_{\text{T}}) = \frac{1}{N_{\text{f}}} \sum_{k} |H(\phi_{\text{R}}, \phi_{\text{T}}; f_{k})e^{j2\pi f_{k}\tau}|^{2}, \quad (2)$$

where τ , $\phi_{\rm R}$ and $\phi_{\rm T}$ are the grid-of-interest for delay, azimuthal DoA and DoD, respectively. Considering a rotating horn channel sounder is deployed for the measurement campaign, the observation, ${\rm H}(\phi_{\rm R},\phi_{\rm T};f_k)$, denotes the measured impulse response when the horn antenna rotates and steers towards the direction $\phi_{\rm R}$ and $\phi_{\rm T}$ at Rx and Tx ends, respectively, which coincide with the angular grids. Since the measurement is conducted for D2D scenario where Tx and Rx are at the same height, only azimuthal angles are taken into account for both DoA and DoD.

However, the ADPS may deviate from the true MPC magnitudes, due to the Fourier grid quantization error when the grids do not coincide with MPCs. The quantization error may lead to errors in both cluster visibility and the modeling statistics. While the angular Fourier grids are fixed due to the selection of $\{\phi_{\rm R}\}$ and $\{\phi_{\rm T}\}$ – $N_{\rm R}$ and $N_{\rm T}$ uniformly distributed directions on $[0,2\pi)$, respectively–the delay grids can be over-sampled by the factor of $N_{\rm os}$ enabling higher delay resolution. This results in an improved angle-delay power spectrum (IADPS), $P_{\rm IADPS} \in \mathbb{R}^{N_{\rm f} \times N_{\rm R} \times N_{\rm T}}$, as the maximal value among every $N_{\rm os}$ consecutive points in the delay domain, to overcome the problem that the true locations of ADPS peaks sit between the original Fourier delay gridpoints.

Since Fourier analysis cannot distinguish between signal and noise, amplitude thresholding is required. For a fair comparison of the different ADPSs, we limit the results to the same dynamic range. The dynamic range is determined by the peak amplitude on one hand, and a noise thresholding level (chosen here to be 12 dB above the average noise power level, to achieve a probability of misinterpreting a noise peak as an MPC is 10^{-7} [18]). We then find that among all the measured ADPSs (both LOS and NLOS), the minimum dynamic range is 35 dB, which is thus the value we use for all thresholding *all* ADPSs, i.e., the subset of Fourier gridpoints whose power is within this dynamic range, named henceforth *MPC taps*, is extracted to build up the MIMO channel model.

III. CLUSTERING

A. Kernel Power Density Method

We next summarize the KPD algorithm [14]. It consists of three main steps.

The first step is the calculation of absolute and relative density of MPC taps. The calculation of the absolute density of a certain tap relies on the total distance measured to its K nearest neighboring taps weighted by a Gaussian kernel in the delay domain, Laplacian kernel in the angular domain, and

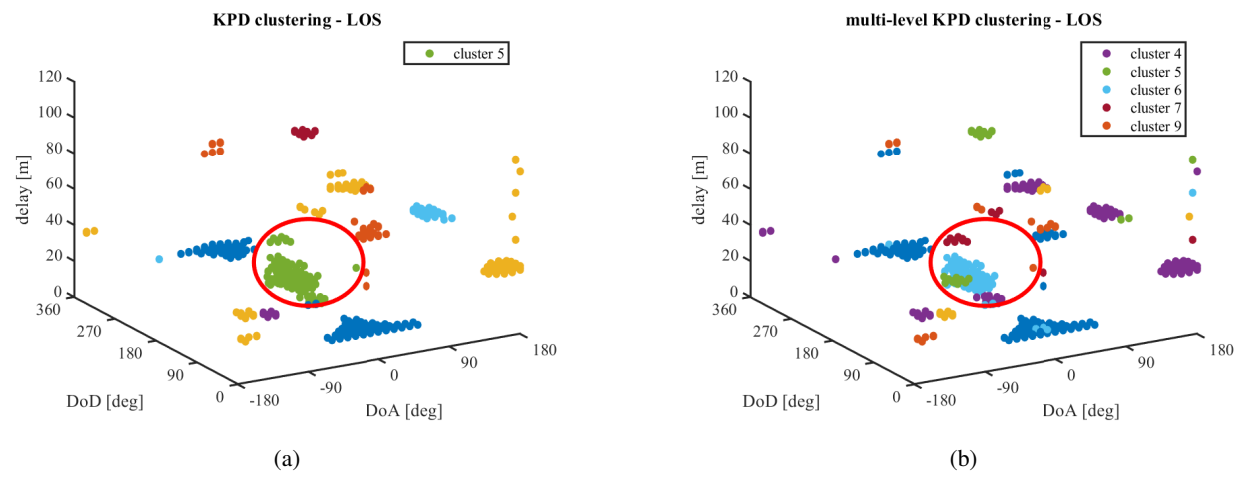


Fig. 1. Clustering comparison of 15-meter LOS outdoor measurement between (a) KPD and (b) multi-level KPD (ML-KPD). Several small clusters, which are observed but not correctly grouped, are clustered and separated properly.

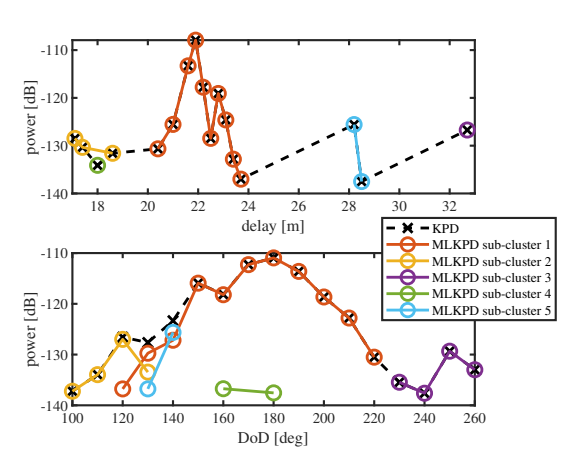


Fig. 2. The total power at delay and DoD angular bin. The KPD clustering result does not match the uni-modal model.

exponentially weighted MPC power [14]. Then the relative density is determined by normalizing by the maximal value among all its nearest components.

In the following step, the taps whose relative density is 1, i.e., whose "importance" is maximum compared to its neighbors, will be identified as *key points*. Considering that the density is higher at the cluster center and lower close to the cluster boundary, the local maxima of taps are the candidates for cluster centroids. Therefore, the key points are automatically initialized as centroids, after which all the points are assigned to one of the key points with the maximal MPC density.

Lastly, all the possible connections between each pair of clusters are explored. If one of the connections between two clusters, measured by the relative density, is greater than a pre-defined threshold, then the clusters can be merged to form a bigger cluster due to the strong connectivity. The clusters remaining after this last step are the final results. The pseudocode of ML-KPD can be found in Alg. 1.

An example of clustering with KPD is shown in Fig. 1(a).

Algorithm 1: Multi-level KPD clustering method

```
1 function ML-KPD(\{\tau\}, \{\phi_{\mathrm{R}}\}, \{\phi_{\mathrm{T}}\})
2 K nearest neighbors, K = \sqrt{M/2};
3 Cluster using KPD;
4 Check separability among N_{\mathrm{C}} clusters;
5 while clusters can be split do
6 Update number of neighbors, K = \sqrt{M_c/2};
7 Cluster using KPD;
8 Check its separability;
9 return All cluster labels
```

Here, we analyze a LOS measurement with 15 m distance between Tx and Rx. Visual inspection demonstrates that the cluster represented by yellow markers (identified in the red circle) is a combination of one big cluster and several small clusters with significant separation in delay and angles. To further analyze this cluster, the powers in each delay- and DoD (as an example for the directional distribution) angularbin are shown in Fig. 2, and denoted by a dashed line with cross markers. It is widely accepted that intra-cluster spectra have a simple and in particular unimodal shape: namely the power as a function of delay follows a singlesided exponential decay, and the angular model is assumed to be either Laplace or von Mises distribution. However, for the intra-cluster power spectra of the cluster extracted by KPD, Fig. 2 shows multiple peaks in both delay and DoD domain. This, in turn, indicates the presence of multiple clusters, confirming the impression from visual inspection of Fig. 1(a). Therefore, this phenomenon verifies the practical limitation of KPD clustering method and motivates its improvement, which will be introduced in the next subsection.

B. Multi-level KPD

The fundamental reason for the aforementioned misclassification phenomenon can be explained as follows. Stronger clusters, measured by total power, may have larger delay and angular spread. In contrast, it is possible to select a

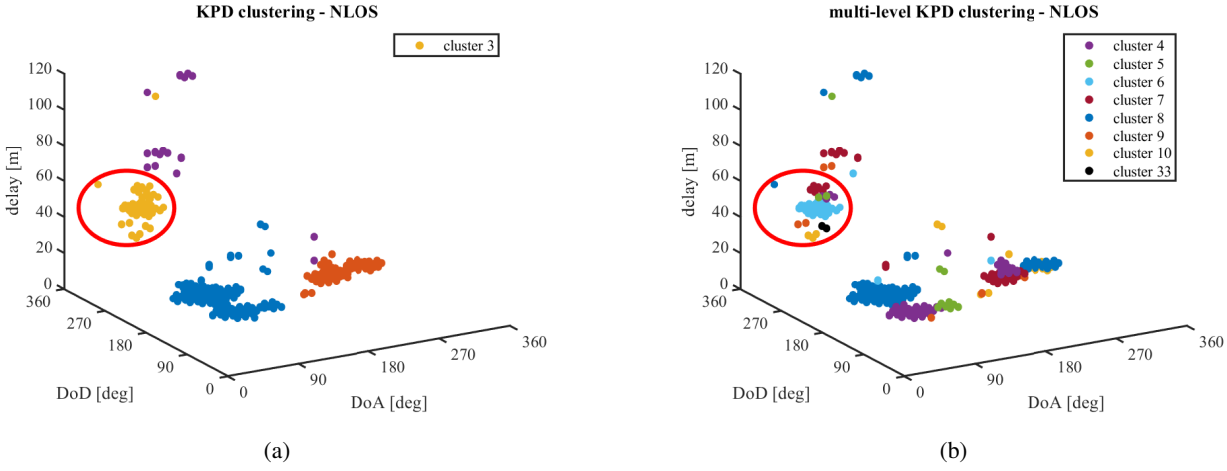


Fig. 3. Clustering comparison of 23-meter NLOS outdoor measurement between (a) KPD and (b) ML-KPD.

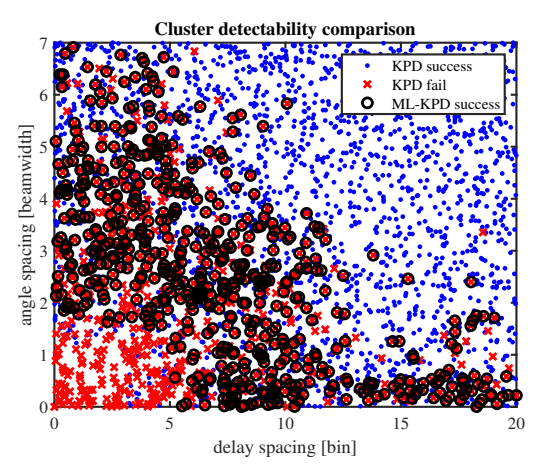


Fig. 4. The detectability comparison between KPD and ML-KPD.

smaller number of taps for weaker clusters. Considering the mechanism of the KPD clustering method, if the number of the selected taps of a certain cluster is less than K, its relative density may be "contaminated" by the surrounding clusters. In particular, the relative density might be significantly *biased* when the weak cluster is closer to one of the stronger clusters. Consequently, it is possible that no key points are initialized for this cluster, leading to an erroneous assignment of the cluster components.

Based on the observation and the analysis, we propose a modification of the KPD method to solve the issue, which we call *ML-KPD*. In this method, KPD will be deployed multiple times to separate a "bulky" cluster and split it into several smaller clusters that satisfy the assumed model. At different levels of the KPD implementation, the values of the nearest neighbors used in computing densities, K, may shrink to improve the *detectability* for smaller clusters.

Firstly, all the extracted taps are fed into KPD methods to cluster into well-separated clusters with the empirical selection $K=\sqrt{M/2}$, where M is the total number of extracted MPC taps. If there are no small clusters within each cluster based on observation, then it is the final result for

clustering.

If the smaller clusters are observed in a certain cluster with M_c taps within, another round of clustering with the KPD method can be applied to it only. Since the current target is the partitioning of a single cluster, the number of the nearest neighbor can be updated by applying a new round of KPD, $K' = \sqrt{M_c/2}$, which may enable the detection of smaller clusters. The whole process is stopped until all the clusters are explored and properly grouped. The additional complexity due to the multiple levels of KPD clustering deployment is upper-bounded by the original KPD complexity multiplied by the number of levels, though in the cases we analyzed the increase in runtime was less than a factor of 3.

Empirically, it usually takes 3 to 4 rounds or levels of KPD application until convergence, i.e., clusters are not further split up. In Fig. 1(b), a successful partition of a big cluster in the red circle in the same LOS measurement location is shown, leading to 5 new sub-clusters. The power in each delay and angular bin for each sub-cluster, denoted by colored circle markers, is compared with the KPD-grouped cluster in Fig. 2. Four of the five clusters satisfy the uni-modal model. For sub-cluster 1, we observe a second peak in both delay and DoD. This may be attributed either to the fading status or could indicate that a further subdivision might be desirable (and the measurements do not allow a distinction of which of those explanations is "true"). However, due to the strong connectivity in delay and angle, we do not consider such a further partition.

Another example comparing the clustering results from KPD and ML-KPD applied to a measurement with Tx and Rx at a distance of 23 m, for a NLOS measurement, is shown in Fig. 3(a) and 3(b).

As measurements do not provide a "ground truth" to allow quantitative assessment of KPD versus multi-level KPD, we further conduct a set of comparison experiments on 4410 different *synthetic* channels. There are two fixed clusters existing in the channel, whose centroids are at 10-th delay bin and 0 deg in the azimuth, denoted by $(10, 0^{\circ})$, and $(30, 300^{\circ})$, respectively, with random disturbance around them. The third cluster's center is varying among the synthetic channels,

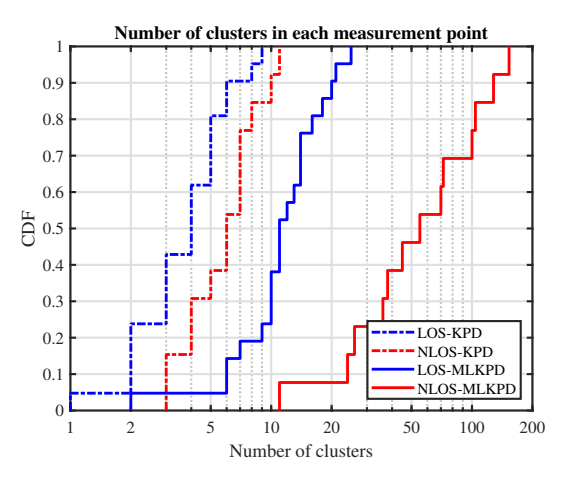


Fig. 5. The CDF of number of clusters.

whose delay with respect to the first cluster is ranging from 0 to 20 delay bins, and the angular spacing ranges from 0 to 7 horn antenna half-power beamwidth (approximately 90 degree). The MPC magnitudes for three clusters are 0, -3, and -10 dB, respectively. With the same MPC tap extraction procedure mentioned in Sec II C, the experiments are used to compare the *detectability* of clustering methods with different parametric separations.

In Fig. 4, the clustering from different methods are shown. The blue dots stand for the cases when three clusters are properly detected. When the "moving" cluster is getting closer to the first cluster in at least one parametric domain, more cases are observed that the clusters are merged with the KPD method, denoted by the red "x" markers. For those cases, we applied with ML-KPD to split up the merged cluster. If all clusters are then separated successfully, a black circle is placed. From Fig. 4, we can observe that the *detectability* of clusters is significantly improved by enabling the additional split-up with adaptive values of K. When two clusters are close enough in all domains, it is almost impossible to separate them, which meets the intuitive expectation.

IV. CLUSTER STATISTICS OF MEASURED D2D CHANNELS

In this section, we present the computed cluster statistics from the D2D outdoor measurement campaign described in Sec. II.A. After the MPC tap extraction from the improved joint beamforming spectrum that is described in Sec II.C, the clustering is conducted using the KPD and ML-KPD method. The statistics of the number of clusters, and of the cluster dispersion, more precisely the intra-cluster rms spreads, in delay and angular domain, are evaluated in this section.

The clusters are all coming from the reflections, diffractions, and scattering interacting with the measurement environment for both LOS and NLOS scenarios, except for the LOS component, which is without interactions. Considering this difference in the underlying propagation mechanism, the LOS cluster is evaluated separately, and the "LOS" scenario excludes the LOS cluster from the computation.

A. Number of Clusters

Fig. 5 shows the cumulative distribution function (CDF) of the number of clusters using KPD and ML-KPD clustering

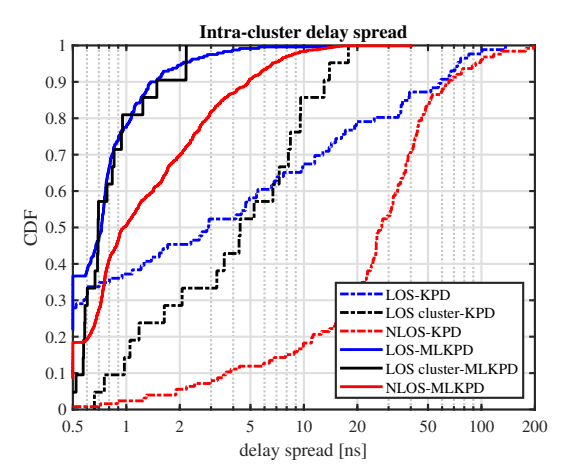


Fig. 6. The CDF of intra-cluster delay spread.

method. The number of clusters increases for both LOS and NLOS scenarios from KPD to ML-KPD, due to the cluster separation effected in multi-level KPD clustering. The NLOS scenario tends to have more clusters, compared to LOS in a similar measurement scenario with the same dynamic range cut-off. We conjecture that this can be attributed to more possible interactions due to the blockage of the boresight path. We furthermore conjecture that for an equal noise floor (instead of an equal dynamic range), the number of clusters for LOS and NLOS would become more similar.

B. Intra-cluster Delay Spread

Intra-cluster delay spread is a statistic to describe the temporal dispersion of rays from the same grouped MPC cluster. The intra-cluster delay spread, DS_c , for cluster c is defined as the square root of the second central moment of the cluster delay profile [4]. In Fig. 6, the intra-cluster delay spread from ML-KPD, denoted by solid lines, shows a significant decrease compared to KPD (denoted by dashed lines). This outcome, delay spread reduction, is expected, as the larger clusters identified by KPD are further partitioned in ML-KPD. LOS clusters have the least delay spread, which is generally less than 3 nanosecond (ns) (approximately 1 meter), due to it containing a single dominant component, in contrast to other clusters. Small-delay clusters can be defined as clusters whose MPCs have similar or even the same delay but extend out in the angular domain. It can be observed that 40% in LOS and 20% in NLOS are weak-delay clusters with less than 0.5 ns delay spread.

C. Intra-cluster Angular Spread

Intra-cluster angular spread is another statistic that is used to describe the dispersion of rays from the same grouped MPC cluster. In this work, we use the unitless angular spread, AS_c , for cluster c as defined by Fleury [19]. Similar to the delay spread, intra-cluster DoA and DoD angular spread from ML-KPD shows a significant decrease compared to KPD due to the further split in ML-KPD as expected. In Fig. 7 and 8, except for the LOS cluster, LOS and NLOS measurements show almost identical angular spread when partitioned by ML-KPD. The small-angle clusters are defined as the cluster with similar or even the same DoA or DoD but only extending

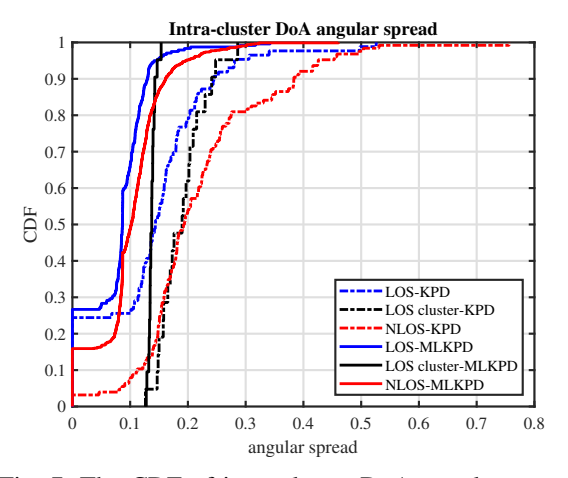


Fig. 7. The CDF of intra-cluster DoA angular spread.

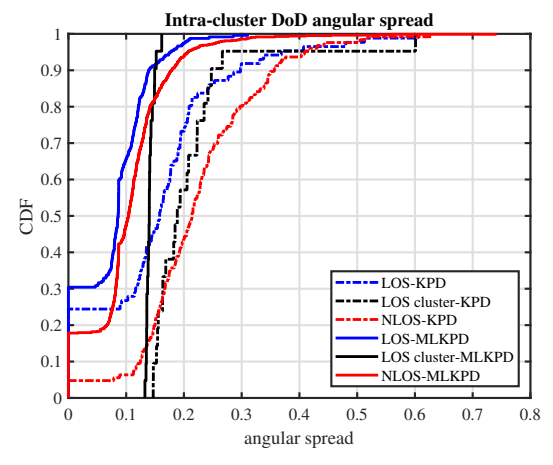


Fig. 8. The CDF of intra-cluster DoD angular spread.

in the delay domain. Analysis shows that 25% in LOS and 15% in NLOS clusters are such weak-delay clusters. Both DoA and DoD angular spread for the LOS cluster is between 0.1 and 0.2, which is approximately between 5 to 10 deg. The LOS cluster angular spread is comparable to the half-power beamwidth of the horn antenna, which is 13 deg [15]. Furthermore, DoA and DoD angular spread distributions are similar, which is intuitive considering that Tx and Rx have the same type of horn antennas, and similar surrounding environments (due to the same height of Tx and Rx.

V. CONCLUSION

In this paper, we analyze the practical limitation of KPD clustering in the analysis of THz D2D outdoor measurements. Due to the fixed number of nearest neighbors in the KPD, smaller clusters cannot be classified properly. Therefore, we improve the "detection ability" by an improved algorithm, namely multi-level KPD, which applies KPD clustering method multiple times, with adaptive nearest neighbors definitions. Experiments with synthetic channels, where ground truth is available, demonstrated the superiority of our new algorithm in resolving weak clusters. We further evaluated the basic statistics—number of clusters in the channel, intra-cluster delay spread, and intra-cluster angular spread—of real-world

LOS and NLOS measurements. While our results focused on urban THz band measurements, a similar approach can be used for any other frequency bands/scenarios.

ACKNOWLEDGMENT

This work was partly supported by the National Science Foundation and by Samsung Research America. The work of J. Gomez-Ponce is partially supported by the Foreign Fulbright Ecuador SENESCYT Program.

REFERENCES

- H. Tataria, M. Shafi, A. F. Molisch, M. Dohler, H. Sjöland, and F. Tufvesson, "6G wireless systems: Vision, requirements, challenges, insights, and opportunities," *Proc. IEEE*, vol. 109, no. 7, pp. 1166–1199, 2021.
- [2] T. S. Rappaport et al., "Wireless communications and applications above 100 GHz: Opportunities and challenges for 6G and beyond," IEEE Access, vol. 7, pp. 78729–78757, 2019.
- [3] T. S. Rappaport, K. A. Remley, C. Gentile, A. F. Molisch, and A. Zajić, "Multipath Component Clustering," in *Radio propagation* measurements and channel modeling: best practices for Millimeter-Wave and Sub-Terahertz Frequencies, ch. 7, pp. 122–152, Cambridge University Press, 2022.
- [4] A. F. Molisch, "Channel Sounding," in Wireless communications, 3rd ed.: from fundamentals to beyond 5G, ch. 9, pp. 183–201, John Wiley & Sons, 2022.
- [5] C. Han et al., "Terahertz wireless channels: A holistic survey on measurement, modeling, and analysis," *IEEE Commun. Surveys Tuts.*, vol. 24, no. 3, pp. 1670–1707, 2022.
- [6] C.-L. Cheng, S. Sangodoyin, and A. Zajić, "THz cluster-based modeling and propagation characterization in a data center environment," *IEEE Access*, vol. 8, pp. 56544–56558, 2020.
- [7] S. Ju, Y. Xing, O. Kanhere, and T. S. Rappaport, "Millimeter wave and sub-terahertz spatial statistical channel model for an indoor office building," *IEEE J. Sel. Areas Commun.*, vol. 39, no. 6, pp. 1561–1575, 2021
- [8] A. A. Saleh and R. Valenzuela, "A statistical model for indoor multipath propagation," *IEEE J. Sel. Areas Commun.*, vol. 5, no. 2, pp. 128–137, 1987
- [9] A. F. Molisch, H. Asplund, R. Heddergott, M. Steinbauer, and T. Zwick, "The COST259 directional channel model-part I: Overview and methodology," *IEEE Trans. Wireless Commun.*, vol. 5, no. 12, pp. 3421–3433, 2006.
- [10] L. Liu et al., "The COST 2100 MIMO channel model," IEEE Wireless Commun., vol. 19, no. 6, pp. 92–99, 2012.
- [11] 3GPP, "Study on channel model for frequencies from 0.5 to 100 GHz," Tech. Rep. TR 38.901 V16.1.0, 3GPP, 2020.
- [12] N. Czink, P. Cera, J. Salo, E. Bonek, J.-P. Nuutinen, and J. Ylitalo, "A framework for automatic clustering of parametric MIMO channel data including path powers," in *IEEE Veh. Technol. Conf.*, pp. 1–5, IEEE, 2006
- [13] M. Ester, H.-P. Kriegel, J. Sander, X. Xu, et al., "A density-based algorithm for discovering clusters in large spatial databases with noise," in Proc. 2nd Int. conf. Knowledge Discovery and Data Mining, vol. 96, pp. 226–231, 1996.
- [14] R. He et al., "A kernel-power-density-based algorithm for channel multipath components clustering," *IEEE Trans. Wireless Commun.*, vol. 16, no. 11, pp. 7138–7151, 2017.
- [15] N. A. Abbasi et al., "THz band channel measurements and statistical modeling for urban D2D environments," *IEEE Trans. Wireless Com*mun., vol. 22, no. 3, pp. 1466–1479, 2022.
- [16] M. Steinbauer, A. F. Molisch, and E. Bonek, "The double-directional radio channel," *IEEE Antennas Propag. Mag.*, vol. 43, no. 4, pp. 51–63, 2001
- [17] N. Czink, The random-cluster model: A stochastic MIMO channel model for broadband wireless communication systems of the 3rd generation and beyond. PhD thesis, TU Vienna, 2007.
- [18] J. Gomez-Ponce et al., "Impact of noisy measurements with fourier-based evaluation on condensed channel parameters," IEEE Trans. Wireless Commun., vol. 23, no. 8, pp. 8136–8152, 2024.
- [19] B. H. Fleury, "First- and second-order characterization of direction dispersion and space selectivity in the radio channel," *IEEE Trans. Inf. Theory*, vol. 46, no. 6, pp. 2027–2044, 2000.